Insights into a historic severe haze event in Shanghai: synoptic situation, boundary layer and pollutants

Chunpeng Leng [a], Junyan Duan [a], Chen Xu [a], Hefeng Zhang [b], Yifan Wang [a], Yanyu Wang [a], Xiang Li [a] *, Lingdong Kong [a], Jun Tao [c], Renjian Zhang [d], Tiantao Cheng [a,e] *, Shuping Zha [e], Xingna Yu [e]

a. Shanghai Key Laboratory of Atmospheric Particle Pollution and Prevention (LAP^3), Department of environmental science and engineering, Fudan University, Shanghai 200433, China;
b. Atmospheric Environment Institute, Chinese Research Academy of Environmental Sciences, Beijing 100012, China;
c. South China Institute of Environmental Sciences, Ministry of Environmental Protection, Guangzhou 510655, China;
d. Key Laboratory of Region Climate-Environment Research for Temperate East Asia, Institute of Atmospheric Physics, Chinese Academy of Sciences, Beijing 100029, China;
e. Key Laboratory of Meteorological Disaster of Ministry of Education，Nanjing University of Information Science and Technology, Nanjing 210044, China;

* Corresponding authors: Tiantao Cheng, Xiang Li
Tel: (86) 21-6564 3230; fax: (86) 21-6564 2080;
Email: ttcheng@fudan.edu.cn, lixiang@fudan.edu.cn

Abstract

A historic haze event, characterized by long duration, large scale and severe pollution, occurred in the Yangtze River Delta (YRD) of China during 1 to 10 December 2013. This haze event significantly influenced air quality throughout the region, especially in urban areas. Aerosol physical, chemical and optical properties were measured in Shanghai. Sometimes the instantaneous particle concentration (e.g. $PM_{2.5}$) exceeded 600 μg m^{-3}. Inorganic water-soluble ions in particles, trace gases and aerosol optical coefficients had a similar tendency to increase evidently from clear to hazy episodes. A combination of various factors contributed to the formation and evolution of the haze event, among which meteorological conditions, local anthropogenic emissions and pollutants are the major factors. High pressure system, calm surface wind and subsidence airflow were responsible for the decrease of planetary boundary layer (PBL) and the accumulation of pollutants. Atmospheric visibility correlated strongly with relative humidity (RH), particle number in size of 600-1400 nm other than particulate water-soluble species and particle mass ($PM_{2.5}$). The particle hygroscopicity plays an important role in atmospheric visibility reduction. The results are somewhat helpful to forecast and eliminate regional atmospheric pollutions in China.

Key words: haze, air pollution, formation mechanism, urban

1. Introduction

Atmospheric aerosols are either emitted from human activities and natural sources or formed by a variety of precursor photochemical reactions. Aerosol exerts great impacts on the earth's radiation balance and climate by directly scattering and absorbing solar and terrestrial radiation, and indirectly modifying cloud and precipitation by acting as cloud condensation nuclei (CCN) (Ramanathan et al., 2001; Andreae et al., 2005; Lohmann et al., 2005). In lower atmospheric layers, aerosol particles can accumulate and result in air pollutions under unfavorable dispersion conditions, and then produce the adverse effects on human health and atmospheric visibility (Wu et al., 2005). Haze is an atmospheric phenomenon that the sky clarity is obscured by dust, smoke and other dry particles, during which atmospheric visibility and relative humidity (RH) are usually below 10 km and 80% (Wu et al., 2006; Xiao et al., 2006; Fu et al., 2008; Bell et al., 2011).

Since World War Ⅱ, haze has occurred in London and Los Angeles due to fast economic development (McNulty, 1968; Lee, 1983; Schichtel et al., 2001). After that, the regions affected by haze have spread to ~~North Africa,~~ Indian Ocean and Asia etc. (Quin and Bates, 2003; Huebert er al., 2003; Du et al., 2011). Until now, the formation and evolution of haze has not been fully understood despite of experiments carried out throughout the world, making it difficult for the governments to take effective

measures to reduce air pollutions (Malm and Day, 2001; Huebert et al., 2003; Wu et al., 2005; Wang et al., 2006b).

China has undergone rapid economic for over 30 years, which releases a large amount of anthropogenic particles and relevant precursors, and forces many cities to suffer from atmospheric pollutions. The increase of haze or hazy days have been observed in the urban environments of northern, eastern, and southwestern China (Sun et al., 2006; Che et al., 2009). Four major regions are mostly influenced by haze in China, i.e. the Jing-Jin-Tang Region (JJT), the Yangtze River Delta (YRD), the Sichuan Base (SCB) and the Pearl River Delta (PRD). The hazy days increased significantly from 70d in 2001 to 144d in 2004 in Guangzhou (Liu et al., 2013). Although the hazy days decreased quickly from 223d in 1982 to 73d in 2005 in Beijing after measures implemented on management of coal demand, motor vehicles, industrial and dust emissions, however, it increased again in 2011 and posed significant effects on human society (Liu et al., 2013). Wang et al. (2006b) compared the aerosol chemical compositions of dusty, hazy and clear days in Beijing, and pointed out that $(NH_4)_2SO_4$, NH_4NO_3 and $Ca(NO_3)_2$ were the major species during hazy days in spring. Sun et al. (2006) found that the concentrations of aerosol elements and water-soluble ions in haze-fog episodes were over 10 times those in clear days in Beijing. The YRD region, one of important economic core areas with large population, high urbanization and advanced

industrialization in China, is facing an inter-annual increase of foggy and hazy days, especially in winter (Tie and Cao, 2009). Ye et al. (2011) discovered the important role of ammonia in haze formation in Shanghai. Du et al. (2011) put insights into summer haze events over Shanghai, and pointed out that the secondary pollutants of increasing sulfate and nitrate were oxidized from large amounts of SO_2 and NO_2 under a high atmospheric oxidation condition. Kang et al. (2013) regarded more accumulation mode particles and higher RH as the main reasons of atmospheric visibility impairment during haze episodes in Nanjing.

To date, available studies on haze in the YRD mainly put efforts to the chemical compositions and physical characteristics of pollutants, but in view of synoptic few focused on the entire process of events at larger scales. It is meaningful to investigate the formation and evolution of regional haze events for useful information to forecast and reduce severe atmospheric pollutions. A winter haze event occurred in the YRD during 1-10 December 2013, known as one historic severe event with features of long duration, large scale and strong pollution. This paper performs a detailed analysis of this serious haze event and gives insights into regional heavy atmospheric pollution in such a fast-developing area.

2. Experiment

2.1 Observation site

The measurement station was mounted on the roof of one building approximately 20m above ground in the campus of Fudan University (31˚18´N, 121˚29´E) in Shanghai, located in the east edge of the YRD region. The site is mainly surrounded by urban residential and commercial zones, approximate 40 km from the East China Sea. Due to Asian monsoon climate, the annual mean precipitation is about 1119 mm, mainly occurring between May and September, and the wind prevails northeasterly in winter and southeasterly in summer. Atmospheric components are likely to originate from local emissions and remote sources (Du et al., 2011). Local time (LT) used in this study is eight hours ahead of UTC.

2.2 Instrument and Measurements

Major water-soluble ions (Na+, K^+, Mg^+, Ca^+, SO_4^{2-}, Cl^-, NO_3^- and NH_4^+) in aerosol particles were measured by an analyzer for Monitoring Aerosols and Gases (MARGA, ADI 2080, Netherlands) at 1 h time resolution. Ambient air is drawn into the sample box with airflow of 1 m^3/h by a pump with mass flow controller (MFC), and the separated gases and aerosols are selectively dissolved and then analyzed by ion chromatography. An internal calibration method, using bromide for the anion chromatograph and lithium for the cation chromatograph, was operated over the whole period to ensure the instrument to identify and measure ion species successfully. The detailed information of sampling, operation and internal calibration can be found elsewhere (Du et al., 2011).

Aerosol particle size distributions in 10nm - 10μm were observed using a high-resolution wide-range particle spectrometer (WPS-1000 XP, MSP). The principle of instrument, combining laser light scattering (LPS), condensation particle counting (CPC) and differential mobility analysis (DMA), has been introduced in detail by Gao et al. (2009). DMA and CPC can effectively count particles in 10nm - 500nm, while LPS is designed to measure particles in 350nm - 10μm. The instrument took 3 min to scan the entire size range completely, 60 channels in DMA and 24 channels in LPS (2 s per channel). Before the campaign, DMA was calibrated using the National Institute of Standards and Technology (NIST) Standard Reference Materials (SRM) 1691 and SRM 1963 Polystyrene Latex (PSL) spheres (mean diameter of 0.269μm and 0.1007μm) to maintain transfer function proper and accurate particle sizing. LPS was calibrated using four NIST traceable sizes of PSL (i.e. 0.701, 1.36, 1.6 and 4.0 μm). Zhang et al. (2010) has described the calibration and operation methodology of WPS in detail.

Black carbon (BC) was measured by an Aethalometer (AE-31, Magee Scientific Co., USA) at 5-min time resolution and 5 l/min airflow rate. According to the strong ability of BC absorption to near-infrared lights, its mass can be determined using the light attenuation at 880 nm and the appropriate specific attenuation cross section proportional to BC (Petzold et al., 1997). The attenuation is calculated based on the intensity difference of reference and sensing beams between light on and off (Hansen et al.,

159 1984; Weingartner et al., 2003). In order to screen the impacts of other
160 absorptive material, the data contaminated by mineral aerosols were
161 excluded from BC measurements. Details for instrument operating and
162 calibrating and data processing can be found in Cheng et al. (2010).

163 Aerosol backscattering profile was measured by a set of micro pulse
164 lidar (MPL-4B) with pulse energy 6-10 μJ and repetition frequency 2500
165 Hz. To date, MPL is utilized widely in the most parts of world as an
166 effective tool for capturing high temporal resolution information of aerosol
167 vertical distributions (Menut et al., 1999; Cohn and Angevine, 2000;
168 Brooks, 2003). Planetary boundary layer (PBL) height is determined by the
169 MPL measurement at the altitude where a sudden decrease of scattering
170 coefficients occurs (Boers and Eloranta, 1986). Instrument calibrations,
171 normalization process, and the analyses of errors propagation and
172 correction uncertainties in MPL processed signal have been described by
173 Campbell et al. (2002), Welton and Campbell (2000) and Welton (2002).

174 Aerosol scattering coefficients (525 nm) were measured using an
175 Aurora-1000 nephelometer (Ecotech Pty Ltd., Australia) at 5-min
176 resolution. The scattering coefficient is calculated by integrating the
177 scattering intensities from angles 7° to 170°. The relative humidity (RH)
178 inside the instrument was retained below 60% to prevent from excessive
179 water vapor entering the chamber. The zero check was operated
180 automatically each day using particle-free air, while the span check was

done every two weeks using R-134a gas.

A CCN counter (CCN-100, DMT, USA) with continuous flow and single column (Roberts and Nenes, 2006; Lance et al., 2006) was employed to monitor CCN concentrations at supersaturations (SS) of 0.2-1.0%. The ambient aerosols were firstly dried by a dryer (activated carbon) to lower relative humidity (RH) below 30%, and subsequently introduced into the counter. The instrument was calibrated for SS using standard $(NH_4)_2SO_4$ particles every three months since 2010. According to the instrument operation manual, regular calibrations were also performed for temperature gradient, input and shear airflows and pressure to maintain stable SS (Leng et al., 2013, 2014a, b). Periodic zero checks were done to ensure counting accuracy for optical particle counter (OPC) inside the CCN counter.

Moreover, two continuous ambient particulate monitors (FH62C14, Thermo) were used to measure $PM_{2.5}$ and PM_{10} (particles in aerodynamic diameter <2.5 μm and <10 μm). The particles are deposited on a glass fiber tape, and then detected by the method of beta attenuation. The particle mass concentration is obtained from the simultaneous measurements of mass and volume of one aerosol sample. An automatic weather station (HydroMet, Vaisala) and a visibility monitor (Vaisala) were employed to measure meteorological variables and atmospheric visibility. The data of hourly-averaged conc. of gases (SO_2, NO_2, CO and O_3) was from the Shanghai Environmental Monitoring Center (SEMC).

3. Results and discussion

3.1 Overview of haze event

3.1.1 Identification of hazy episode

It has been widely accepted that the key criterion for discerning a haze event is an apparent decrease of atmospheric visibility less than 10 km and ambient relative humidity (RH) below 80% lasting for several hours (Fu et al., 2008; Du et al., 2011). When 80% < RH < 90%, the event is referred to as a complex of haze-fog co-occurring or transition (Leng et al., 2014a), and it is also classified into hazy episode in the present study.

Figure 1a depicts the temporal variations of hourly $PM_{2.5}$, PM_{10}, atmospheric visibility and meteorological factors from 1 to 10 December 2013. On the whole, atmospheric visibility mostly declined to below 10 km, and RH hardly reached 90%. The haze event constituted of several sub-episodes, marked by gray areas in Figure 1a. It was clear that Shanghai suffered from a long-term haze event until 10 December, and subsequently loosened when atmospheric visibility improved and the clean sky took control afterwards. In fact, these hazy sub-episodes approximately accounted for 70% of the entire period, with mean atmospheric visibilities of 5.65 km for the former compared to 29.45 km for the rest (30%).

On a larger scale, this haze event caused a historic atmospheric pollution, and attacked the most parts of central and eastern China. $PM_{2.5}$ in many cities exceeded 150 $\mu g\ m^{-3}$, and some more than 300-500 $\mu g\ m^{-3}$ even 600

225 μg m^{-3}, as expected, this event will produce one serious problem to people's
226 health at that time (Cao et al., 2012).

227 **3.1.2 Meteorological conditions**

228 Precipitation did not appear during the whole campaign. For most of the
229 period (Figure 1b and 1c), ambient RH and temperature correlated
230 negatively and showed an evident diurnal pattern, varying in the ranges of
231 20-87% and 6-17 °C, respectively. The hazy episodes were usually
232 characterized by higher RH and lower temperature, while the clean periods
233 often corresponded to lower RH and higher temperature. The main reason
234 is that high temperature can strengthen the vertical dispersion of pollutants
235 due to thermal effects, and high RH can facilitate aerosol scattering due to
236 hygroscopicity. The wind was weak (< 2 m s^{-1}, 87%) during the hazy
237 episodes until 9 December, but in the following day it became strong (>4
238 m s^{-1}) and conductive to the dispersion of air pollutants due to transiting
239 cold front (Figure 1b and 1c). The wind direction was basically northeast
240 or southeast during the clean periods, originating from marine areas.
241 However, the wind normally turned into northwest when the haze took over,
242 which will probably bring a large quantity of pollutants from inland areas
243 and to some extent cause pollutant accumulation in downwind.

244 **3.1.3 Particulate mass concentration**

245 $PM_{2.5}$ and PM_{10} were employed to represent ambient particulate mass
246 burden per volume in the atmospheric boundary layer. $PM_{2.5}$ and PM_{10}

247 instantaneously ranged within 50-600 μg m^{-3} and 55-680 μg m^{-3} throughout
248 the whole campaign (Figure 1a), and both of them significantly rose during
249 the hazy episodes with averages of 315 and 333 μg m^{-3}, compared to 112
250 and 134 μg m^{-3} in the clean periods. On the other hand, the ratios of
251 $PM_{2.5}/PM_{10}$ varied between 0.54 and 0.97, and averaged at 0.88, 0.93, 0.8
252 in total, hazy and clean periods, indicating that the fine particles are major
253 contributors to particle mass.

254 Interestingly, both $PM_{2.5}$ and PM_{10} reached their peaks of 600 and 680
255 μg m^{-3} as new historic records on 6 December, approximately 14 times
256 higher than the Grade I criteria of the National Ambient Air Quality
257 Standard of China (50 μg m^{-3} for PM_{10}), and 24 times the World Health
258 Organization Air Quality Guidelines (25 μg m^{-3} for $PM_{2.5}$). Other cities in
259 the YRD showed a similar tendency and high $PM_{2.5}$ along with this haze
260 event, such as 226 μg m^{-3} in Hangzhou, 230 μg m^{-3} in Nanjing and 260 μg
261 m^{-3} in Hefei (Figure 2). The numerous measurements earlier in Shanghai
262 during the last decade showed much lower values. For example, Wang et
263 al. (2006a) observed that $PM_{2.5}$ varied within 17.8-217.9 μg m^{-3} and
264 averaged at 94.6 μg m^{-3}. According to the Shanghai Environmental Bulletin
265 2010 (www.envir.gov.cn/law/bulletin/2010/), the annual average of PM_{10}
266 in 2009 was about 79 μg m^{-3}. Leng et al. (2014a) reported $PM_{2.5}$ average of
267 143 μg m^{-3} during hazy episode and 46 μg m^{-3} during clear episode in
268 November 2010. They also observed that $PM_{2.5}$ varied in 10-210 μg m^{-3} in

January 2011 and 10-130 μg m^{-3} in April 2012, respectively (Leng et al., 2013, 2014b). In addition, compared to Beijing as another megacity in China, He et al. (2001), Sun et al. (2004) and Liu et al. (2013) monitored $PM_{2.5}$ extremes of 357 μg m^{-3} from July 1999 to September 2000, 349 μg m^{-3} in winter from 2002 to 2003, and 220 μg m^{-3} in September 2011. Briefly, the particulate mass burden was extremely high in this haze event, and so serious air pollution, unsuitable for human beings (Liu et al., 2013), must cause a formidable environmental disaster.

3.1.4 High aerosol columnar loading

Aerosol optical depth (AOD), retrieved from MODIS employing the algorithm well introduced by Li et al. (2005), can be acted as a good indicator of aerosol loading in the whole atmosphere. Figure 3 depicts a full feature of AOD spatial distribution and its day-to-day development during the haze event. Briefly, the covering region of high AODs (>0.5) was generally spreading out a big domain, about most of the South China. High AODs originated from the YRD and the SCB, then extended to the central South China, the southwestern China and even the south of the JJT region, and moved to the YRD area in the end.

In the most serious days, AODs were as high as 1.00-1.25 on 5-8 December. According to the records of the Ministry of Environmental Protection of China (http://www.zhb.gov.cn/), many cities in the upwind areas (e.g. Nanjing, Wuxi, and Suzhou) had higher AODs up to 1.5 and

AQI over 500, implying that the inflow of pollutants to Shanghai is inevitable to contribute to the pollution. In addition, the weak circulation (Sect. 3.2.1) normally led to the build-up of pollutant pooling and contributed to the haze event formation.

3.1.5 Aerosol optical properties

Figure 4 shows a temporal series of BC, aerosol scattering coefficient Sc (525 nm), and aerosol absorption coefficient Ab (532 nm). Based on the assumption that the averaged mixing state of BC is uniform, the Ab coefficient is indirectly calculated from measured BC according to the following equation (Yan et al., 2008),

$$Ab=\alpha\times[BC] \qquad (1)$$

where [BC] represents BC mass concentration, and α is BC absorption efficiency which is adopted as 8.28 g m^{-2} in this paper. This value was obtained from the inter-comparison experiment performed in southern China previously, and was within the variance range of various source regions (Bergin et al., 2001; Bond and Bergstrom, 2006; Yan et al., 2009; Zhao et al., 2013). The aerosol scattering and absorption coefficients in combination determine its extinction ability, namely aerosol extinction coefficient (Ex=Ab+Sc).

Basically, BC, Sc and Ab had the same tendency to increase in the hazy episodes, and reached to their max values at 0:00 LT on 6 December, i.e. 35 μg m^{-3}, 2.8×10^{3} M m^{-1} and 290 M m^{-1}, approximately 4-5 times higher

than their mean values in the clean periods (8.3 μg m^{-3}, 643 M m^{-1} and 58 M m^{-1}). The enhancement of aerosol optical properties largely contributed to atmospheric visibility decreasing, which correspondingly deteriorated to its minimum of 50 m at the same moment (Figure 1). The mean aerosol single scattering albedo (SSA=Sc/Ex, 532nm) was expectedly low at 0.89, indicating more absorptive species existing in the particle group.

3.1.6 Condensation nuclei and cloud condensation nuclei

Aerosol size distribution was analyzed in detail to shed some light on its relationship with haze. Figure 5a presents a time series of aerosol size spectra and integrating particle size-resolved number concentrations (N_{CN}). N_{CN} showed an evident diurnal pattern with two peaks corresponding to the traffic rush hours, and appeared higher mean and instantaneous values in the hazy episodes (15000 and 25000 cm^{-3}) than the clean periods (9500 and 17000 cm^{-3}). Generally, ambient aerosol particles in higher loading mainly distributed in a wider size range over the hazy episodes than the clean periods, 20-200 nm for the former and 20-100 nm for the latter. The averaged aerosol number size distribution is shown in Figure 5b. About 67% of particles fell in the size range of 10-100 nm, and the percent further increased to 91% when enlarged to 10-200 nm. This result is in good agreement with the early observations that urban ambient aerosols mainly distribute in ultrafine size section (Woo et al., 2001; Gao et al., 2007), slightly higher than 62% reported in Nanjing and 61% in Atlanta, a little

lower than 72% in Eastern Germany and significantly lower than 94% in Taicang (Woo et al., 2001; Tuch et al., 1997; Gao et al., 2009; Kang et al., 2013).

Cloud condensation nuclei (CCN) constitutes an important fraction of atmospheric aerosol population, and can indirectly influence global climate change through modifying the microphysical and radiative properties and lifetime of cloud (IPCC, 2013). It tends to reduce cloud droplet size and then suppress the wet precipitation in shallow and short-lived clouds (Lohmann and Feichter, 2005). Previous studies in Shanghai have found that CCN number concentration (N_{CCN}) and aerosol activity promotes effectively during the polluted periods (Leng et al., 2013, 2014). In north India, Ritesh et al. (2007) observed a significant impact of winter haze on N_{CCN}. To gather more information about CCN during haze, hourly N_{CCN} at SS of 0.2-1.0% were plotted as a function of time in Figure 6. As expected, N_{CCN} increased with SS, i.e. 3800-10000 cm^{-3} at SS 0.2% and 4000-16000 cm^{-3} at SS 1.0%, and exhibited bimodal daily distributions. Agreed well with N_{CN}, N_{CCN} greatly enhanced during the hazy episodes, about 1.6-1.8 folds (on varying SS) of that during the clean periods.

3.1.7 Aerosol chemical species

A key for understanding haze is to characterize both aerosol composition and trace gases quantitatively (Du et al., 2011). As important components of atmospheric particles, water-soluble inorganic ions are thought to be a

357 significant contributor to atmospheric visibility impairment (Kang et al.,
358 2013).

359 The time series of hourly water-soluble inorganic ions in $PM_{2.5}$,
360 including Na^+, K^+, Mg^+, Ca^+, SO_4^{2-}, Cl^-, NO_3^- and NH_4^+, and gaseous
361 pollutants such as SO_2, NO_2, CO and O_3 from 1 to 10 December are
362 presented in Figure 7. Aerosol water-soluble ions, highly coinciding with
363 particulate mass, showed higher contents in the hazy episodes than the
364 clean periods. Totally, the mean concentrations of these ions were
365 comparable to that monitored earlier in Shanghai (Yao et al., 2002; Wang
366 et al., 2006a; Du et al., 2011). The mean concentrations of these ions were
367 in sequence of NO_3^->SO_4^{2-}>NH_4^+>Cl^->K+>Na^+>Mg^{2+}, and their
368 contributions to $PM_{2.5}$ were 11.7%, 7.7%, 6.7%, 1.5%, 0.6%, 0.3% and
369 0.08%, respectively, slightly higher than that observed in haze pollutions
370 in Nanjing and Guangzhou (Tan et al., 2009; Kang et al., 2013). Overall,
371 the integrated water-soluble ions accounted for 28.5% of $PM_{2.5}$, higher than
372 the dust event but significantly lower than the biomass burning event
373 observed in Nanjing (Zhang et al., 2012).

374 Gaseous species play a vital role in atmospheric process by acting as
375 precursors or mediums of photochemical reactions. Among them, O_3 has
376 been widely known as the products of photochemical reactions between
377 volatile organic compounds (VOCs) and nitrogen oxides (NO_X) with the
378 participation of heat and sunlight, while SO_2, NO_2, and CO are mainly

emitted from biomass, fuel and coal burning (Seinfeld and Pandis, 2006). Seen in Figure 7, the measured gaseous pollutants behaved an increasing trend during the hazy episodes, with one exception of O_3 probably due to consumption by oxidation of NO and other species (Liu et al., 2013).

NO_3^- and SO_4^{2-} are products of NO_2 and SO_2 due to atmospheric oxidation, hence their concentrations strongly depended on related gaseous precursors and oxidation rate in the atmosphere. Two equations are used to estimate the extent of this transformation process (Sun et al., 2006):

$$NOR=nNO_3^-/(nNO_3^-+nNO_2) \quad (3)$$

$$SOR=nSO_4^{2-}/(nSO_4^{2-}+nSO_2) \quad (4)$$

Where NOR and SOR means nitrogen oxidation rate and sulfur oxidation rate, n refers to molar concentration. It can be easily deduced that larger NOR and SOR would generate more atmospheric aerosols, and atmospheric photolysis reaction of SO_2 would take place if the oxidation rate exceeds 0.1 (Ohta and Okita, 1990). In this study, NOR and SOR were always higher than 0.1 with averages of 0.14 and 0.27, respectively, suggesting that atmospheric oxidation of NO_2 and SO_2 contributed significantly to the formation of particulate matter. The mean NOR was comparable to that in Nanjing (0.16) during a long-lasting haze event but apparently lower than in Guangzhou (0.24), while the SOR was much higher that in Nanjing (0.13) but comparable to the value in Guangzhou (0.26) (Tan et al., 2009; Kang et al., 2013). Meanwhile, NO_2 surpassed SO_2

so strong with a mass ratio of 1.53, hence more atmospheric H_2O_2 and OH would be removed via reactions with NO_2, and the formation of SO_4^{2-} would be greatly suppressed due to the competition effect (Poppe et al., 1993). Furthermore, the mass ratio of ambient nitrate to sulfate (NO_3^-/SO_4^{2-}) can help to track the relative importance of stationary versus mobile sources of nitrate and sulfur in the atmosphere (Yao et al., 2002). The stationary emission dominates in the sources of SO_2 and NO_2 if the ratio is less than 1.0, otherwise SO_2 and NO_2 mainly come from traffic activities (Huebert et al., 1988). Shanghai has been experiencing an increasing trend of NO_3^-/SO_4^{2-} because of the very fast development of motor vehicles over the past decade (Yao et al., 2002; Wang et al., 2006a; Fu et al., 2008). Therefore, more contribution of pollutants from mobile sources is expected to the local pollutions. The mean NO_3^-/SO_4^{2-} during this haze event was 1.53, comparable to our early measurement in 2010 (1.61), but significantly higher than those observed in haze events in Guangzhou (1.02) and Nanjing (0.84 and 1.05) (Tan et al., 2009; Kang et al., 2013; Leng et al., 2013). The traffic-emitted SO_2 and NO_2 preponderating their stationary sources so conspicuous illustrated that the increasing traffic activities is one of main reasons for visibility degradation.

3.2 Formation and evolution of haze event

3.2.1 Atmospheric circle and synoptic situation

During winter time, the YRD region is often influenced by cold air from

north, such as cold high pressure and cold front, and surface temperature inversion takes place sometimes (Chen et al., 2003; Liu et al., 2013). Under those conditions, atmospheric mixing and dispersion are basically weak in favor of pollutant accumulation, hence haze or fog easily occurs (Xu et al., 2011; Zhao et al., 2013).

The mean geopotential height field at 500 hPa revealed that during 1-10 December a long wave adjustment happened over the middle and high latitude of Eurasia. On 1 to 5, the atmospheric circulation in this region was representative of two troughs and one ridge, and these troughs were located in the west of the Balkhash lake and the north of Northeast China and a wide ridge of high pressure existed between them (Figure 8). On 6, the circulation situation changed to two troughs and two ridges, and these troughs were located in the west of Lake Baikal and the east of Asia. However, over the central and southern China, there were flat westerly flows in most times with smaller radial degree and fast-moving short-wave troughs and ridges. During the haze event, the central and southern China was mainly under the stable westerly, and the YRD was affected by it. Additionally, at 700 hPa, the shear lines generated continuously and moved eastwards, and the difference between temperature and dew point mostly exceeded 4 ℃, and the weak westerly and wind convergence appeared over the areas covered by haze clouds. At 850 hPa, the YRD was influenced by anticyclonic ring in most of time, wind speed smaller even static, and in

445 view of temperature, this region was in one weak warm structure,
446 isotherms relatively flat.

447 The surface weather maps at 6:00 (UTC) from 3-8 December are shown
448 in Figure 9. A slowly migrating anti-cyclone (high-pressure) overlaid the
449 YRD region and possibly caused a build-up of pollution due to the
450 concomitant subsidence airflow and relatively stagnant conditions. The
451 high pressure dominating this area also indicated aloft airflow convergence
452 and surface divergence, which in turn would subside and restrict PBL
453 development, and accordingly limit the convection of pollutants by
454 trapping them within a shallow altitude. Unfavorable ambient temperature
455 posed another adverse effect on the thermal dynamic development of PBL
456 height. The small pressure gradients over the YRD would horizontally
457 suppress the air circulation at large scales because of low wind speed
458 mostly below 2 m s^{-1} during the hazy episodes. Under those favorable
459 situations, e.g. stable synoptic condition and calm wind, atmospheric
460 pollutants were easily to accumulate within the surface atmospheric layer
461 which ultimately led to severe urban air pollution. On the other hand, the
462 YRD was sometime controlled by low pressure periphery and trough, and
463 the pressure gradient was relatively weak. Although the low pressure was
464 conducive to the rise of air masses, the vertical movement of upper and
465 lower levels of the atmosphere was too weak to produce the effective
466 dispersion of air pollutants and then result in pollution. Furthermore, the

effect of ambient aerosols uptaking water vapor would effectively enhance their ability of scattering or absorbing solar radiation and damage atmospheric visibility eventually. The high ambient RH (60-80%) over this haze process indeed made a rich supply of water vapor for enhancing aerosol hygroscopic growth and was mostly responsible for the atmospheric visibility impairment. Normally, external forces such as high wind or rainfall are necessary to interrupt the stable situation and favor the diffusion of pollutants.

Over the target region (30° 40' ~31° 53'), during the haze event, the vertical winds almost were less than 0.4 Pa/s between 500 hPa and surface, and it was less than 0.2 Pa/s at 700 hPa, implying that the vertical exchange of air parcels between the upper and lower atmospheric layers is very weak. Near the ground, the vertical velocity of winds was positive, and the relative vorticity was zero or negative value in most of time, demonstrating that airflow was prevailed in downdraft at the bottom of the atmosphere. Moreover, the temperature profile of sounding data revealed that the strong inversions occurred in 5 days with relatively low heights, so atmospheric convection and turbulence were inhibited, and then the blocked diffusion in vertical direction caused pollutant accumulation near the surface.

In summary, atmospheric pollutants were restricted within shallow layer, favorable for visibility impairment due to the dominance of weak high pressure system with low pressure gradients, subsidence airflow,

unfavorable PBL height and meteorological situation. In good agreement with our study, Wu et al. (2005) reported that descending air motion and weak horizontal wind produced significantly high particle concentrations during a severe haze event in Guangzhou. Also in the YRD area, Fu et al. (2008) found that high pressure system responsible for stagnant conditions was the major reason of high pollution events. The stable synoptic condition and its long duration was indeed viewed as one of the most important factors ruling the formation and evolution of this haze event.

3.2.2 Impacts of air mass pathways

HYSPLIT-4 model, developed by the Air Resources Laboratory (ARL) of the National Oceanic and Atmospheric Administration (NOAA) of USA (Draxler and Rolph, 2003), was employed to compute 48 h air mass backward trajectories at 500 m height, starting at 0:00 UTC and 12:00 UTC for each day. By doing so, we can identify and compile a full view of the possible source regions of pollutants.

According to those calculated trajectories plotted in Figure 10, three types of air mass pathways were determined in summary. Firstly, the air mass wandered inside the region with shallow atmospheric boundary layer, accounting for 60% of total trajectories, which was in good agreement with stable synoptic condition during the hazy episodes. This situation facilitates the accumulation of atmospheric pollutants and ultimately results in haze formation. Secondly, the subsidence flow from high altitude

511 with minor horizontal movement, accounting for 30% of trajectories,
512 dominated and brought in temporal clear sky between the hazy episodes on
513 2, 3 and 8 December. Thirdly, the air mass, originating from the northern
514 inland China at high altitude, fast travelled southerly across the Northern
515 China Plain (NCP) and the Eastern Region of China (ERC), and finally
516 arrived in Shanghai over a long distance on 10 December, accounting for
517 10% of trajectories. They are helpful to dilute the atmospheric pollutants
518 and then end this haze event. Most possibly, a combination of local
519 emissions and long-distance transportation of remote emissions exerts the
520 joint effects to the pollutants during the haze event.

521 **3.2.3 Reduction of PBL height**

522 PBL plays a vital role in determining the vertical dispersion of air
523 pollutants that are emitted naturally or artificially from the Earth surface
524 (Kim et al., 2007; Liu et al., 2013). Decreasing height of PBL can normally
525 hold the pollutants within the shallow surface layer, suppress the vertical
526 atmospheric dilution and ultimately cause regional environment shrouded
527 by pollution (Kim et al., 2007). In Shanghai, several field measurements
528 have monitored that PBL height is usually low during hazy episodes (Leng
529 et al., 2014b; Zhang et al., 2015). By utilizing the normalized Lidar
530 backscatter signal at 532 nm, the PBL retrieval at 30-sec resolution was
531 derived in this study, and the time-height series was plotted in red line in
532 Figure 11. Overall, PBL height was negatively correlated with atmospheric

visibility with R^2 of 0.63, and averaged at 1.3 km during the clean periods and 0.6 km during the hazy episodes. From midday on 5 to the night on 6 December, the height of PBL decreased to 400 m lasting more than 30 hours, and $PM_{2.5}$ during this period enhanced to over 600 $\mu g\ m^{-3}$, 5.4 times of the average of the clean periods. The lower PBL heights will retain more pollutants in the surface layer and cause the city surrounded by haze.

In theory, PBL basically evolves as a function of atmospheric thermal and dynamic factors, e.g. air temperature and wind speed (Liu et al., 2013). In fact, there is a feedback between atmospheric aerosol loading and PBL height. Briefly, the more ambient aerosols accumulate, the less solar radiation reaches to surface, which inevitably poses a disadvantageous effect on surface air temperature as well as a positive impact on ambient RH, and further restricts the development of PBL. The low PBL height in turn forces the accumulation of aerosol particles in the high RH and shallow atmosphere, and ultimately degrade atmospheric visibility (Liu et al., 2013). Otherwise, more solar radiation arrives at the ground in case of clean sky, under those conditions the air temperature and PBL height increase while the ambient RH drops, which is unfavorable to the haze formation. This scientific issue involves many complicated atmospheric processes remaining poorly understood as well as deserving further study. As mentioned in Sect. 3.2.1 and 3.2.2, the YRD region was undergoing a large scale of weak high pressure with surface air moving slowly during

555 the campaign. The air temperature retained at a low level which was not
556 conductive to the development of PBL, thereby heavy air pollution took
557 place and eventually resulted in visibility degradation. In short, the low
558 PBL height is helpful for the increase of aerosol particles, hence favors the
559 occurrence of haze event.

560 **3.2.4 Aerosol composition and hygroscopicity**

561 As important components of ambient particles, particle-phase water-
562 soluble inorganic ions generally account for 30% of particulate matter in
563 urban atmosphere, and are considered as a great contributor to the
564 atmospheric visibility impairment because they hugely determine the
565 ability of aerosol particles to uptake water vapor (Hillamo et al., 1998;
566 Andrews et al., 2000; Chow et al., 2006; Seinfeld and Pandis, 2006). Also,
567 they are essential participants in the formation, growth and evolution of
568 nanoparticles by providing significant potential of surface chemical
569 reactions (Wang et al., 2006b). In Shanghai, sulfate and nitrate have been
570 evidently identified as great contributors to the occurrence of heavy
571 particulate pollution events (Wang et al., 2006b; Sun et al., 2006; Fu et al.,
572 2008), and NH_3 plays a vital role in the enhancement of particulate sulfate
573 and nitrate (Ye et al., 2011).

574 When ambient RH is high, those aerosols that are more hydrophilic can
575 grow in diameter via uptaking water vapor, and through this way they can
576 increase their ability of scattering light and cause atmospheric visibility

impairment (Tang, 1996). A kappa value κ, describing particle hygroscopicity, was firstly introduced by Petters and Kreidenweis (2007) and employed here to investigate its relationship with haze formation. Assuming ambient aerosols are well internal-mixed, the effective integrated κ can be obtained through weighting their chemical compound volume factions,

$$\kappa = \sum_i \varepsilon_i \kappa_i \qquad (5)$$

where ε_i is the volume fraction of chemical compounds in particles, and κ_i is the effective κ of individual chemical composition. Equation (5) has been widely used and described elsewhere in detail (Petters and and Kreidenweis., 2008; Yue et al., 2011; Leng et al., 2014a, 2014b). In this study, aerosol particle compositions were classified into three categories, and κ_i and ε_i for individual composition are listed in Table 1, of which "others" refers to PM_{10}-(SO_4^{2-}+NO_3^-+NH_4^++Cl^-+Na^+), and is viewed as a chemical compound with κ_i=0 (Yue et al., 2011). Figure 11 provides the time series of hourly-averaged kappa values, with higher κ during the hazy episodes (0.22) and lower κ during the clean periods (0.15), indicating that aerosols are basically more hygroscopic responsible for haze occurrence during the pollution period.

With the aim of better understanding the potential contribution of individual water-soluble ions, BC and ambient RH to atmospheric visibility impairment, we run nonlinear regression analysis and the results

were plotted in Figure 12. The correlation between atmospheric visibility and individual ions, BC and $PM_{2.5}$ was not so impressive with R^2 from 0.11 to 0.22. However, it became more significant in view of ambient RH with R^2 of 0.41. The result suggests that the atmospheric visibility impairment is less driven by water-soluble ions but largely induced by hygroscopicity, in consistent with Tang (1996) and Roeland et al. (2014).

3.2.5 Aerosol size spectra

Atmospheric aerosol particles are usually divided into four classes according to their size distribution, i.e. nucleation mode (<25 nm), Aitken mode (25-100 nm), accumulation mode (100-1000 nm), and coarse mode (>1000 nm) (Zhang et al., 2010). The ability to determine the amount of visible light scattered by atmospheric aerosols relies strongly on their number size distributions, of which accumulation mode plays the major role yet coarse and nucleation mode exert a minor contribution (Cheng et al., 2008b). Numerous studies have observed the inter-relationship between atmospheric visibility and aerosol number size distribution (Cheng et al., 2008; Roeland et al., 2014). To be more specific, Kang et al. (2013) reported that the expected reciprocal relationship was found only between atmospheric visibility and aerosols in 600-1400 nm instead of other sizes.

Accordingly, aerosol particles were classified into three categories, i.e. 10-600 nm, 600 nm-1.4 μm and 1.4-10 μm. By doing so, their nonlinear

621 regression analysis with atmospheric visibility was computed and the
622 results were given in Figure 13. As expected, no significant correlation was
623 derived between atmospheric visibility and aerosol size of 10-600 nm and
624 1.4-10 μm, whereas aerosols in 600 nm-1.4 μm indeed controlled
625 atmospheric visibility to a great extent with R^2 of 0.70, which further
626 improved to 0.73 if we combined aerosol hygroscopic potential well
627 determined by its size-resolved composition. In this study, aerosol number
628 concentrations in 600 nm-1.4 μm were on average 110 cm^{-3} during the hazy
629 episodes and 43 cm^{-3} during the clean periods. The atmospheric visibility
630 was so dependent on aerosol number size distribution and its impairment
631 during the hazy episodes was mostly caused by the enhancement of aerosol
632 concentration in 600 nm-1.4 μm.

633 ## 4. Summary and conclusion

634 A historic haze event was fully analyzed for the temporal variations of
635 aerosol optical, physical and chemical properties and meteorological
636 conditions, as well as the formation and evolution mechanism. During the
637 event, atmospheric visibility decreased dramatically, while particle burden,
638 water-soluble inorganic ions, aerosol scattering and absorption coefficients
639 increased evidently. In particular, particulate mass burden produced a new
640 historic record by exceeding 600 μg m^{-3}.

641 Many factors in combination drove the formation and evolution of this
642 severe haze event. For most of the measured period, the YRD was under

the control of a slowly migrating anti-cyclone to result in subsidence airflow and relatively stagnant conditions. The subsidence airflow suppressed vertical mixing and favored the accumulation of air pollutants within the shallow atmospheric layer. Moreover, the calm surface wind subsidence airflow was not constructive to the horizontal dispersion of air pollutants which further promoted the haze formation. In summary, the significant increase of regional pollutants from anthropogenic emissions was the basic cause of this haze formation, and the unfavorable meteorological conditions played as the external reason.

Acknowledgements

This research is supported by the National Key Technology R&D Program of Ministry of Science and Technology (2014BAC16B01), the National Natural Science Foundation of China (41475109), and partly by the Jiangsu Collaborative Innovation Center for Climate Change, and the Key Laboratory for Aerosol-Cloud-Precipitation of China Meteorological Administration (KDW1401) and the Laboratory of Meteorological Disaster of Ministry of Education (KLME1416).

Referrence

Andrews, E., Saxena, P., Mussara, S., Hildemann, L. M., Koutrakis, P., McMurry, P. H., Olmez, I., and White, W. H.: Concentration and composition of atmospheric aerosols from the 1995 SEAVS experiment and a review of the closure between chemical and gravimetric measurements, Journal of the Air&Waste Management Association, 50, 648-664, 2000.

Bell, M. L., Cifuentes, L. A., Davis, D. L., Cushing, E., and Telles, A. G.: Gouveia, N. Environmental health indicators and a case study of air pollution in Latin American cities, Environ. Res., 111, 57-66, 2011.

Bergin, M., Cass, G. R., Xu, J., Fang, F., Zeng, L. M., Yu T., Salmon, L. G., Kiang, C. S., Tang, X. Y., Zhang, Y. H., and Chameides, W. L.: Aerosol radiative, physical, and chemical properties in Beijing during June 1999, J. Geophys. Res., 106, 17969–17980, 2001.

Boers, R., and Eloranta, E.W.: Lidar measurements of the atmospheric entrainment zone and the potential temperature jump across the top of the mixed layer, Bound.-Lay. Meteorol., 34, 357–375, 1986.

Bond, T. C. and Bergstrom R. W.: Light Absorption by Carbonaceous Particles: An Investigative Review, Aerosol Sci. Technol., 40, 27–47, 2006.

Brooks, I. M.: Finding boundary layer top: application of a wavelet covariance transform to lidar backscatter profiles, J. Atmos. Ocean. Tech.,

687 20, 1092–1105, 2003.
688 Campbell, J. R., Hlavka, D. L., Welton, E. J., Flynn, C. J., Turner, D. D.,
689 Spinhirne, J. D., Scott, V. S., and Hwang, I. H.: Full-time, eye-safe cloud
690 and aerosol lidar observation at atmospheric radiation measurement
691 program sites: Instruments and data processing, J. Atmos. Ocean Technol.,
692 19, 431–442, 2002.
693 Cao J, Xu H, Xu Q, et al. Fine particulate matter constituents and
694 cardiopulmonary mortality in a heavily polluted Chinese city, J.
695 Environmental health perspectives, 120, 373-378, 2012.
696 Che, H. Z., Zhang, X. Y., Li, Y., Zhou, Z. J., Qu, J. J., Hao, X. J.: Haze
697 trends over the capital cities of 31 provinces in China, 1981–2005, Theor.
698 Appl. Climatol., 97, 235–242, 2009.
699 Chen, L. W. A., Chow, J. C., Doddridge, B. G., Dickerson, R. R., Ryan, W.
700 F., and Mueller, P. K.: Analysis of a summertime $PM_{2.5}$ and haze episode
701 in the mid-Atlantic region, J. Air Waste Mange. Assoc., 53, 946–956,
702 2003.
703 Cheng, T. T., Han, Z. W., Zhang, R. J., Du, H. H., Jia, X., Wang, J. J., and
704 Yao, J. Y.: Black carbon in a continental semi-arid area of Northeast China
705 and its possible sources of fire emission, J. Geophys. Res., 115, D23204,
706 doi:10.1029/2009JD013523, 2010.
707 Cheng, Y. F., Wiedensohler, A., Eichler, H., Heintzenberg, J., Tesche, M.,
708 Ansmann, A., Wendisch, M., Su, H., Althausen, D., Herrmann, H., Gnauk,

709 T., Bruggemann, E., Hu, M., and Zhang, Y. H.: Relative humidity
710 dependence of aerosol optical properties and direct radiative forcing in
711 the surface boundary layer at Xinken in Pearl River Delta of China: An
712 observation based numerical study, Atmos. Environ., 42, 6373–6397,
713 2008a.
714 Cheng, Y. F., Wiedensohler, A., Eichler, H., Su, H., Gnauk, T., Br ¨
715 uggemann, E., Herrmann, H., Heintzenberg, J., Slanina, J., Tuch, T., Hu,
716 M., and Zhang, Y. H.: Aerosol optical properties and related chemical
717 apportionment at Xinken in Pearl River Delta of China, Atmos. Environ.,
718 42, 6351–6372, 2008b
719 Chow, J. C., Chen, L. W. A., Watson, J. G., Lowenthal, D. H., Magliano,
720 K. A., Turkiewicz, K., and Lehrman, D. E.: $PM_{2.5}$ cheimcal composition
721 and spatiotemporal variability during the California regional
722 PM10/PM2.5 air quality study (CRPAQS), J. Geophys. Res., 111,
723 D10S04, 2006.
724 Cohn, S. A., Angevine, W. M.: Boundary layer height and entrainment
725 zone thickness measured by lidars and wind-profiling radars, J. Appl.
726 Meteorol., 39, 1233–1247, 2000.
727 Draxler, R. R. and Rolph, G. D.: HYSPLIT (Hybrid Single-Particle
728 Lagrangian Integrated Trajectory) Model access via NOAA ARL READY
729 Website (http://www.arl.noaa.gov/ready/hysplit4.htm), NOAA Air
730 Resources Laboratory, Silver Spring, MD, 2003.

731 Du, H. H., Kong, L. D., Cheng, T. T., Chen, J. M., Du, J. F., Li, L., Xia, X.
732 G., Leng, C. P., and Huang, G. H.: Insights into summertime haze
733 pollution events over Shanghai based on online water-soluble ionic
734 composition of aerosols, Atmos. Environ., 45, 51311-5137, 2011.
735 Fu, Q. Y., Zhuang, G. S., Wang, J., Xu, C., Huang, K., Li, J., Hou, B., Lu,
736 T., and Streets, D. G.: Mechanism of formation of the heaviest pollution
737 episode ever recorded in the Yangtze River Delta, China, Atmos. Environ.,
738 42, 2023–2036, 2008.
739 Gao, J., Wang, T., Zhou, X. H., Wu, W. S., and Wang, W. X.: Measurement
740 of aerosol number size distributions in the Yangtze River delta in China:
741 formation and growth of particles under polluted conditions, Atmos.
742 Environ., 43, 829–836, 2009.
743 Hansen, A. D. A., Rosen, H., and Novakov, T.: The aethalometer-an
744 instrument for the real-time measurement of optical absorption by aerosol
745 particles, Sci. Total Environ., 36, 191–196, 1984.
746 Hillamo, R., Allegrini, I., Sparapani, R., and Kerminen, V.M.: Mass size
747 distributions and precursor gas concentrations of major inorganic ions in
748 Antarctica aerosol, International Journal of Environmental Analytical
749 Chemistry, 71, 357-369, 1998.
750 Huebert, B. J., Bates, T., Russell, P. B., Shi, G. Y., Kim, Y. J., Kawamura,
751 K., Carmichael, G., and Nakajima, T.: An overview of ACE-Asia:
752 Strategies for quantifying the relationships between Asian aerosols and

753 their climatic impacts, J. Geophys. Res., 108, 1–20, 2003.
754 Huebert, B. J., Wang, M. X., Lv, W. X.: Atmospheric nitrate, sulfate,
755 ammonium and calcium concentrations in China, Tellus B
756 http://dx.doi.org/10.1111/j. 1600-0889.1988.tb00296.x., 1988.
757 IPCC: Climate Change 2013: The Physical Science Basis. Contribution of
758 Working Group I to the Fifth Assessment Report of the Intergovernmental
759 Panel on Climate Change, edited by: Joussaume, S. Penner, J., and
760 Tangang, F., IPCC, Stockholm, 2013.
761 Kang, H. Q., Zhu, B., Su, J. F., Wang, H. L., Zhang, Q. C., and Wang, F.:
762 Analysis of a long-lasting haze episode in Nanjing, China, Atmos. Res.,
763 120-121, 78-87, 2013.
764 Kim, S. W., Yoon, S. C., Won, J. G., and Choi, S. C.: Ground-based remote
765 sensing measurements of aerosol and ozone in an urban area: A case study
766 of mixing height evolution and its effect on ground-level ozone
767 concentrations, Atmos. Environ., 41, 7069-7081, 2007.
768 Lance, S., Medina, J., Smith, J. N., and Nenes, A.: Mapping the operation
769 of the DMT Continuous Flow CCN counter, Aerosol Sci. Tech., 40, 242–
770 254, 2006
771 Leng, C. P., Cheng, T. T., Chen, J. M., Zhang, R. J., Tao, J., Huang, G. H.,
772 Zha, S. P., Zhang, M. G., Fang, W., Li, X., and Li, L.: Measurements of
773 surface cloud condensation nuclei and aerosol activity in downtown
774 Shanghai, Atmos. Environ., 69, 354–361, 2013.

775 Leng, C. P., Zhang, Q., Zhang, D. Q., Xu, C., Cheng, T. T., Zhang, R. J.,
776 Tao, J., Chen, J. M., Zha, S. P., Zhang, Y. W., Li, X., and Kong, L. D.:
777 Variations of Cloud Condensation Nuclei (CCN) and Aerosol Activity
778 during Fog-Haze Episode: a Case Study from Shanghai, Atmos. Chem. &
779 Phys., 14, 12499-12512, 2014a.
780 Leng, C. P., Zhang, Q., Tao, J., Zhang, H. F., Zhang, D. Q., Xu, C., Li, X.,
781 Kong, L. D., Cheng, T. T., Zhang, R. J., Yang, X., Chen, J. M., Qiao, L.
782 P., Lou, S. R., Wang, H. L., and Chen, C. H.: Impacts of New Particle
783 Formation on Aerosol Cloud Condensation Nuclei (CCN) Activity in
784 Shanghai: Case Study, Atmos. Chem. & Phys., 14, 11353-11365, 2014b.
785 Lee, D. O.: Trends in summer visibility in London and Southern England
786 1962–1979, Atmos. Environ., 17, 151–159, 1983.
787 Li, C., Lau, K. H., Mao, J., and Chu, D. A.: Retrieval, validation and
788 application of the 1-km aerosol optical depth from MODIS measurements
789 over Hong Kong, IEEE T. Geosci. Remote, 43, 2650–2658, 2005.
790 Liu, X. G., Li, J., Qu, Y., Han, T., Hou, L., Gu, J., Chen, C., Yang, Y., Liu,
791 X., Yang, T., Zhang, Y., Tian, H., and Hu, M.: Formation and evolution
792 mechanism of regional haze: a case study in the megacity Beijing, China,
793 Atmos. Chem. Phys., 13, 4501-4514, 2013.
794 Lohmann, U. and Feichter, J.: Global indirect aerosol effects: a review,
795 Atmos. Chem. Phys., 5, 715–737, doi:10.5194/acp-5-715-2005, 2005.
796 Malm, W. C. and Day, D. E.: Estimates of aerosol species scattering

797 characteristics as a function of relative humidity, Atmos. Environ., 35,
798 2845-02860, 2001.
799 McNulty, R. P.: The effect of air pollutants on visibility in fog and haze at
800 New York city, Atmos. Environ., 2, 625–628, 1968.
801 Menut, L., Flamant, C., Pelon, J., and Flamant, P. H.: Urban boundary-
802 layer height determination from lidar measurements over the Paris area,
803 Appl. Optics, 38, 945–954, 1999.
804 Ohta, S., Okita, T.: A chemical characterization of atmospheric aerosol in
805 Sapporo, Atmos. Environ., 24A, 815-822, 1990.
806 Petters, M. D. and Kreidenweis, S. M.: A single parameter representation
807 of hygroscopic growth and cloud condensation nucleus activity, Atmos.
808 Chem. Phys., 7, 1961–1971, doi:10.5194/acp-7-1961-2007, 2007.
809 Petzold, A., Kopp, C., and Niessner, R.: The dependence of the specific
810 attenuation cross-section on black carbon mass fraction and particle size,
811 Atmos. Environ., 31, 661–672, 1997.
812 Poppe, D., Wallasch, M., Zimmermann, J.: The dependence of the
813 concentration of OH on its precursors under moderately polluted
814 conditions: a model study, J. Atmos, Chem., 16, 61-78, 1993.
815 Ritesh, G., Christina, H., Menas. Kafatos., Si-Chee. T.: Influences of winter
816 haze on fog/low cloud over the Indo-Gangetic plains, J. Geophys. Res.,
817 112, D05207, doi:10.1029/2005JD007036, 2007.
818 Roberts, G. C. and Nenes, A.: A continuous-flow streamwise thermal-

819 gradient CCN chamber for atmospheric measurements, Aerosol Sci.
820 Tech., 39, 206–221, 2006.
821 Schichtel, B. A., Husar, R. B., Falke, S. R., and Wilson, W. E.: Haze trends
822 over the United States, 1980–1995, Atmos. Environ., 35, 5205–5210,
823 2001.
824 Sun, Y. L., Zhuang, G. S., Wang, Y., Han, L. H., Guo, J. H., Dan, M., Zhang,
825 W. J., Wang, Z. F., and Hao, Z. P.: The air-borne particulate pollution in
826 Beijing-Concentration, composition, distribution and sources, Atmos.
827 Environ., 38, 5991–6004, 2004.
828 Sun, Y. L., Zhuang, G. S., Tang, A. H., Wang, Y., and An, Z. S.: Chemical
829 characteristics of $PM_{2.5}$ and PM_{10} in haze-fog Episodes in Beijing,
830 Environ. Sci. Technol., 40, 3148–3155, 2006
831 Quinn, P. K. and Bates, T.: North American, Asian, and Indian haze:
832 Similar regional impacts on climate?, Geophys. Res. Lett., 30, 1555,
833 doi:10.1029/2003GL016934, 2003.
834 Seinfeld, J. H., and Pandis, S. N.: Atmospheric Chemistry and Physics:
835 From Air Pollution to Climate Change, second ed. John Wiley & Sons,
836 New York, USA, 57-58 and 381-383, 2006.
837 Tan, H. H., Duan, J. C., He, K. B., Ma. Y. L., Duan, F. K., Chen, Y., Fu, J.
838 M.: Chemical characteristics of PM2.5 during a typical haze episode in
839 Guangzhou, J. Environ. Sci., 21, 774-781, 2009.
840 Tang, I. N.: Chemical and size effects of hygroscopic aerosols on light

841 scattering coefficients, J. Geophys. Res., 101, 19245–19250, 1996.
842 Tie, X. X., Wu, D., and Brasseur, G.: Lung cancer mortality and exposure
843 to atmospheric aerosol particles in Guangzhou, China, Atmos. Environ.,
844 43, 2375–2377, 2009.
845 Wang, Y., Zhuang, G. S., Zhang, X. Y., Huang, K., Xu, C., Tang, A. H.,
846 Chen, J. M., An, Z. S.: The ion chemistry, seasonal cycle, and sources of
847 $PM_{2.5}$ and TSP aerosol in Shanghai, Atmos. Environ., 40, 2935-2952,
848 2006a.
849 Wang, Y., Zhuang, G. S., Sun, Y. L., and An, Z. S.: The variation of
850 characteristics and formation mechanisms of aerosols in dust, haze, and
851 clear days in Beijing, Atmos. Environ., 40, 6579–6591, 2006b.
852 Weingartner, E., Saathoff, H., Schnaiter, M., Streit, N., Bitnar, B., and
853 Baltensperger, U.: Absorption of light by soot particles: determination of
854 the absorption coefficient by means of aethalometers, J. Aerosol Sci., 34,
855 1445-1463, 2003.
856 Welton E.J., Voss K.J., Quinn P. K., Flatau P. J., Markowicz K., Campbell
857 J. R., Spinhirne J.D., Gordon H.R., Johnson, J. E., Measurements of
858 aerosol vertical profiles and optical properties during INDOEX 1999
859 using micropulse lidars, J. Journal of Geophysical Research:
860 Atmospheres, 107, doi: 10.1029/2000JD000038, 2002.
861 Welton E.J., Campbell J.R., Micropulse lidar signals: Uncertainty analysis,
862 J. Journal of Atmospheric and Oceanic Technology, 19, 2089-2094, 2002.

Woo, K. S., Chen, D. R., Pui, D. Y. H., McMurry, P. H.: Measurements of Atlanta aerosol size distributions: observations of ultrafine particle events, Aerosol Sci. Technol., 34, 75-87, 2001.

Wu, D., Bi, X., Deng, X., Li, F., Tan, H., Liao, G., and Huang, J.: Effects of atmospheric haze on the deterioration of visibility over the Pearl River Delta, Acta Meteorol. Sin., 64, 510–517, 2006.

Wu, D., Tie, X., Li, C., Ying, Z., Lau, A. K.-H., Huang, J., Deng, X., and Bi, X.: An extremely low visibility event over the Guangzhou region: a case study, Atmos. Environ., 39, 6568–6577, 2005.

Xiao, F., Brajer, V., and Mead, R. W.: Blowing in the wind: the impact of China's Pearl River Delta on Hong Kong's air quality, Sci. Total Environ., 367, 96–111, 2006.

Xu, W. Y., Zhao, C. S., Ran, L., Deng, Z. Z., Liu, P. F., Ma, N., Lin, W. L., Xu, X. B., Yan, P., He, X., Yu, J., Liang, W. D., and Chen, L. L.: Characteristics of pollutants and their correlation to meteorological conditions at a suburban site in the North China Plain, Atmos. Chem. Phys., 11, 4353–4369, doi:10.5194/acp-11-4353-2011, 2011.

Yao, X. H., Chan, C. K., Fang, M., Cadle, S., Chan, T., Mulawa, P., He, K. B., Ye, B. M.: The water-soluble ionic composition of $PM_{2.5}$ in Shanghai and Beijing, China, Atmos. Environ., 36, 4223-4234, 2002.

Ye, X. N., Ma, Z., Zhang, J. C., Du, H. H., Chen, J. M., Chen, H., Yang, X., Gao, W., and Geng, F. H.: Important role of ammonia on haze formation

885 in Shanghai, Environ. Res. Lett., 6, doi: 10.1088/1748-9326/6/2024019,
886 2011.
887 Yue, D. L., Hu, M., Zhang, R. J., Wu, Z. J., Su, H., Wang, Z. B., Peng, J.
888 F., He, L. Y., Huang, X. F., Gong, Y. G., and Wiedensohler, A.: Potential
889 contribution of new particle formation to cloud condensation nuclei in
890 Beijing, Atmos. Environ., 45, 6070–6077, 2011.
891 Zhang, M., Wang, X. M., Chen, J. M., Cheng, T. T., Wang, T., Yang, X.,
892 Gong, Y. G., Geng, F. H., and Chen, C. H.: Physical characterization of
893 aerosol particles during the Chinese New Year's firework events, Atmos.
894 Environ., 44, 5191–5198, 2010.
895 Zhang, Q. C., Zhu, B., Su, J. F., Wang, H. L.: Characteristcs of aerosol
896 water-soluble inorganic ions in three types air-pollution incidents of
897 Nanjing City, Environ. Sci., 33(6), 1944-1951, 2012 (in Chinese).
898 Zhao, P. S., Dong, F., He, D., Zhao, X. J., Zhang, X. L., Zhang, W. Z., Yao,
899 Q., and Liu, H. Y.: Characteristics of concentrations and chemical
900 compositions for PM2.5 in the region of Beijing, Tianjin, and Hebei,
901 China, Atmos. Chem. Phys., 13, 4631–4644, doi:10.5194/acp-13-4631-
902 2013, 2013
903 Zhao, X. J., Zhao, P. S., Xu, J., Meng, W., Pu, W. W., Dong, F., He, D., and
904 Shi, Q. F.: Analysis of a winter regional haze event and its formation
905 mechanism in the North China Plain, Atmos. Chem. Phys., 13, 5685-5696,
906 2013.

Table 1. Effective hygroscopicity parameters (κ) and densities of the three category compositions.

Species	Data source	κ	Density (g cm^{-3})
Sulfate & nitrate	SO_4^{2-}+NO_3^-+NH_4^+	0.6	1.7
Sodium chloride	Cl^-+Na^+	1	2.2
Insoluble compounds	Others	0	2.0

Figure captions:

Figure 1. (a)Temporal variations of $PM_{2.5}$, PM_{10} and atmospheric visibility (vis) measured in Shanghai from 1 to 10 December 2013. The dash line is vis at 10 km.(b) and (c) show temporal variations of meteorological parameters from 1 to 10 December 2013.

Figure 2. Temporal variations of PM2.5 in Hangzhou, Nnajing and Hefei (a) and their mean concentrations from 1 to 10 December 2013.

Figure 3. Aerosol optical depth (AOD) at 550 nm from MODIS over the YRD region at 6:00 (UTC) from 1 to 10 December 2013 (http://modis.gsfc.nasa.gov/).

Figure 4. Temporal variations of black carbon (BC) concentration, aerosol scattering (Sc) and absorptive (Ab) coefficients from 1 to 10 December 2013.

Figure 5. (a) Time series of 4-min mean aerosol number size spectra and aerosol number concentration (pink line) and (b) averaged aerosol number size distribution from 5 to 10 December 2013.

Figure 6. Time series of 1 h mean CCN concentration (N_{CCN}) at supersaturations (SS) of 0.2-1.0% from 6 to 10 December 2013.

Figure 7. Temporal variations of chemical species in particles from 1 to 10 December 2013.

Figure 8. Atmospheric circulation situation at 500 hPa and 850 hPa from 3 to 6 December 2013.

Figure 9. Surface weather maps from 3 to 8 December 2013. The black star denotes the measurement site(http://qixiangxinxifabupingtai.ejinqiao.com).

Figure 10. Air mass 48-h backward trajectories arriving at Shanghai from 1 to 10 December 2013. A new trajectory is started at 0:00 (UTC) and calculated every 24 h.

Figure 11. Time series of 1-h mean kappa value (i.e. κ) and 5-min mean PBL height from 1 to 10 December.

Figure 12. Scatter plots of RH, BC, $PM_{2.5}$ and inorganic ions in particles versus atmospheric visibility.

Figure 13 Scatter plots of aerosol number concentrations in ranges of 0.01-0.6 μm, 0.6-1.4 μm and 1.4-10 μm, and aerosol number concentration multiplied by particle hygroscopcity (kappa value, κ) versus atmospheric visibility.

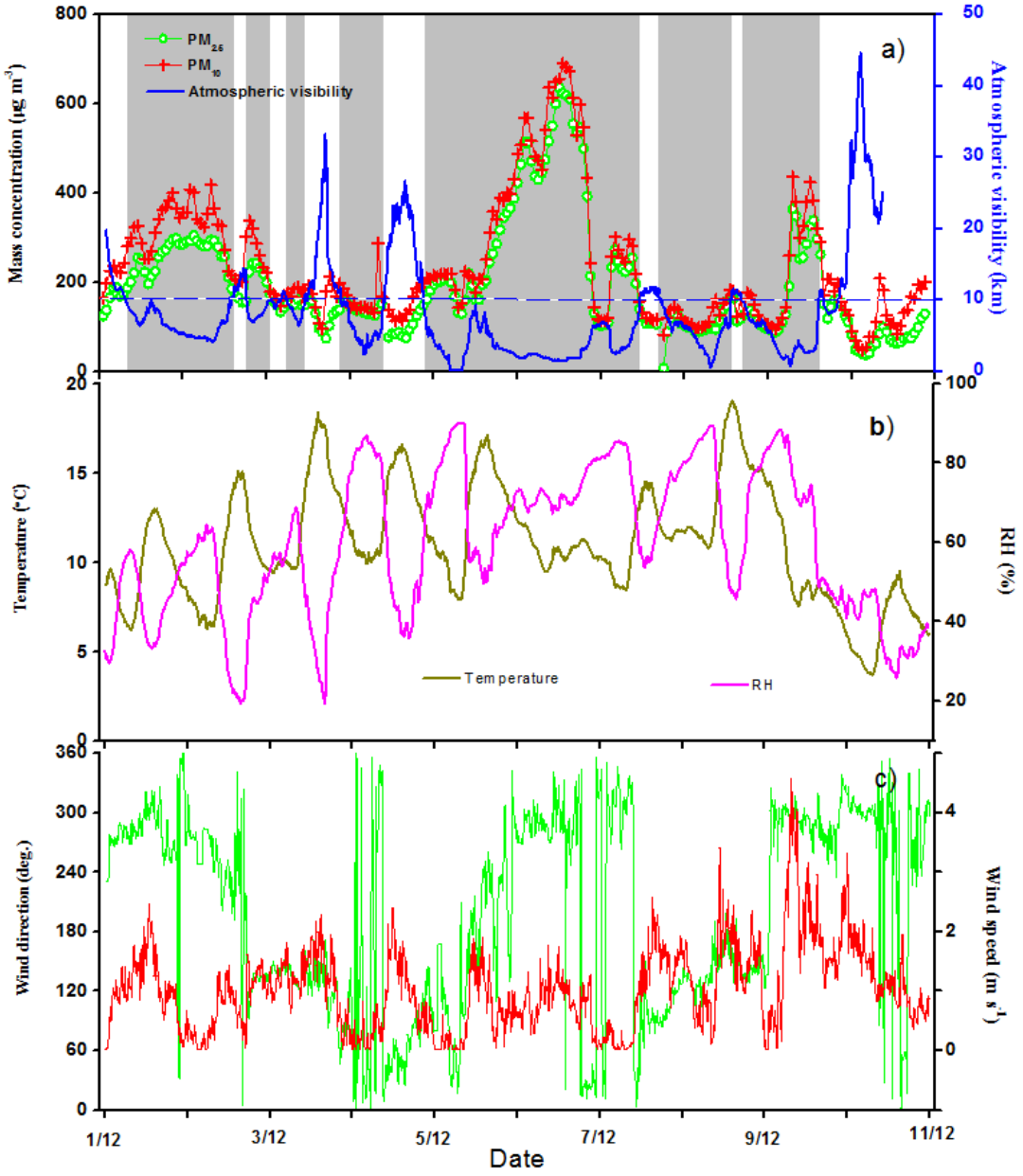

Figure 1(a) Temporal variations of $PM_{2.5}$, PM_{10} and atmospheric visibility (vis) measured in Shanghai from 1 to 10 December 2013. The dash line is vis. at 10 km. (b) and (c) show temporal variations of meteorological parameters from 1 to 10 December 2013.

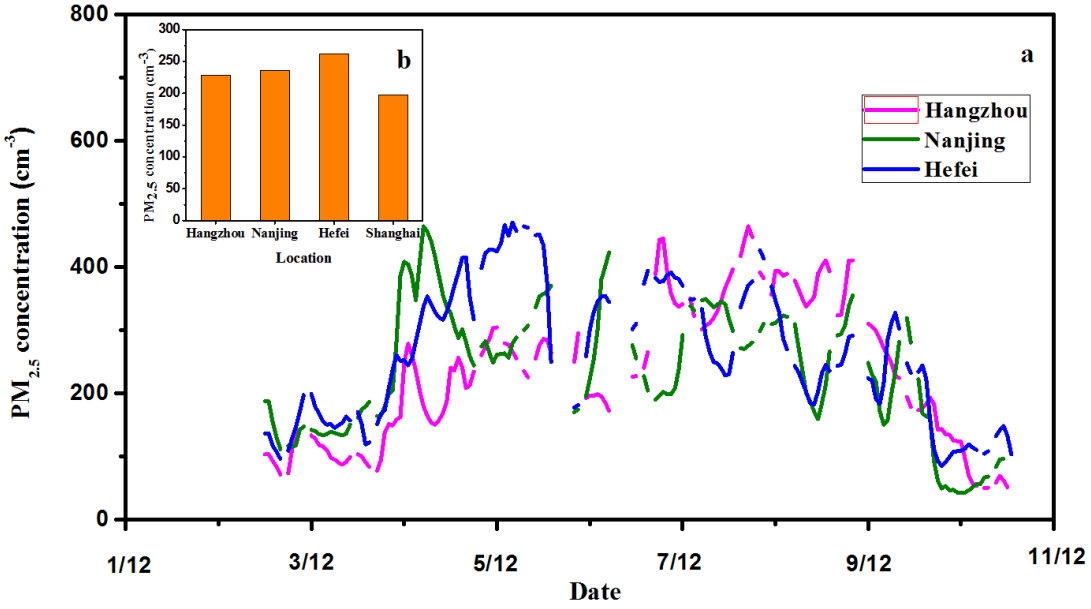

Figure 2 Temporal variations of $PM_{2.5}$ in Hangzhou, Nanjing and Hefei (a) and their mean concentrations (b) from 1 to 10 December 2013.

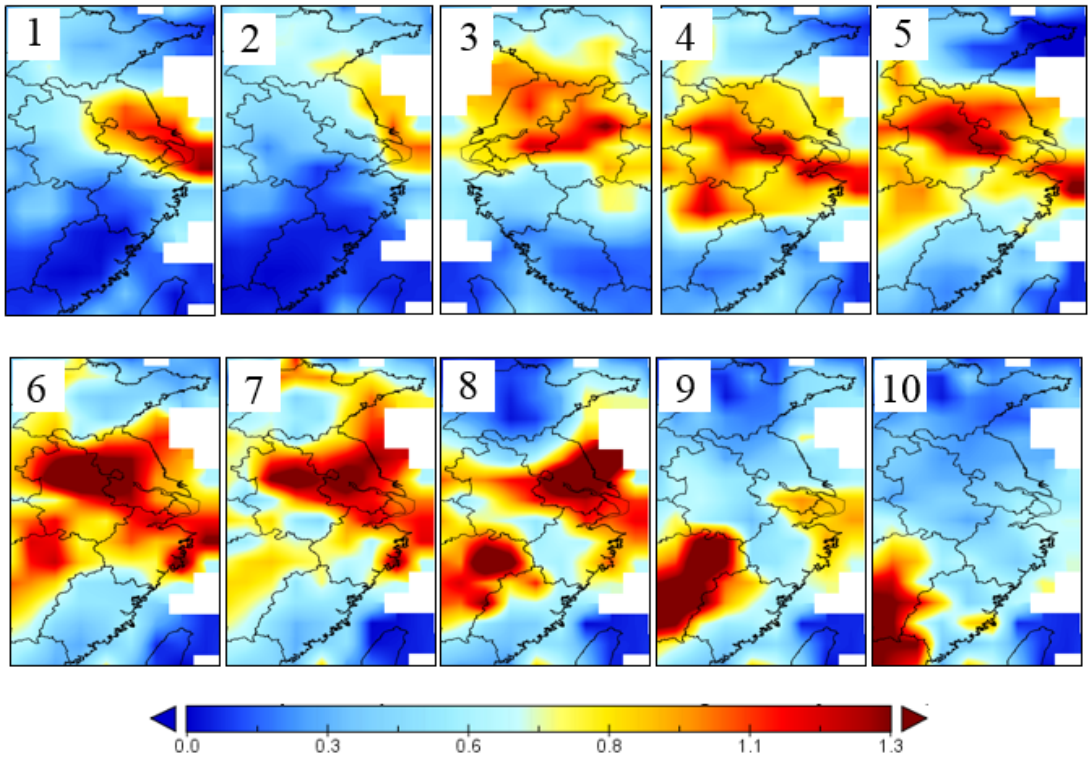

Figure 3 Aerosol optical depth (AOD) at 550 nm from MODIS over the YRD region at 6:00 (UTC) from 1 to 10 December 2013 (http://modis.gsfc.nasa.gov/).

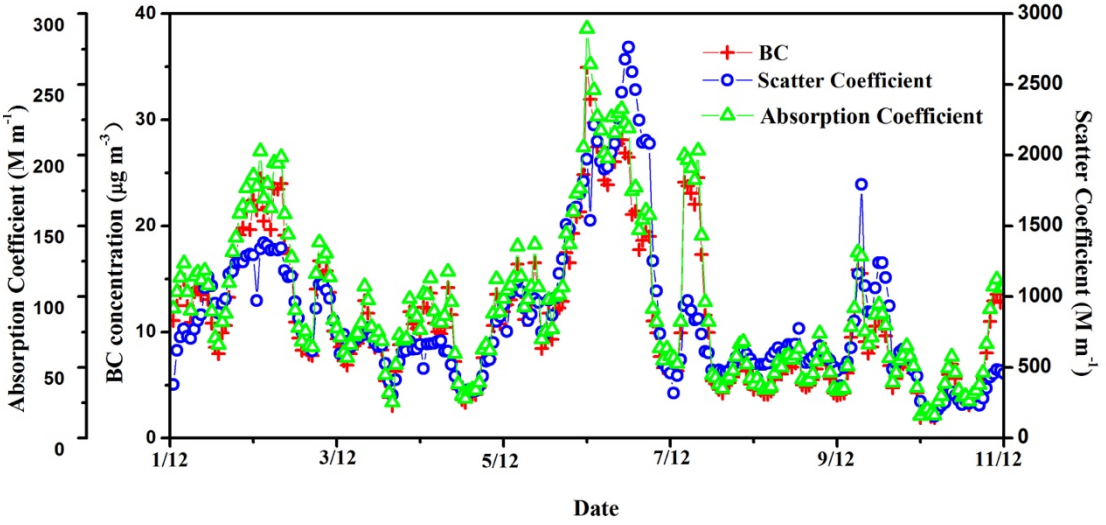

Figure 4 Temporal variations of black carbon (BC) concentration, aerosol scattering (Sc) and absorptive (Ab) coefficients from 1 to 10 December 2013.

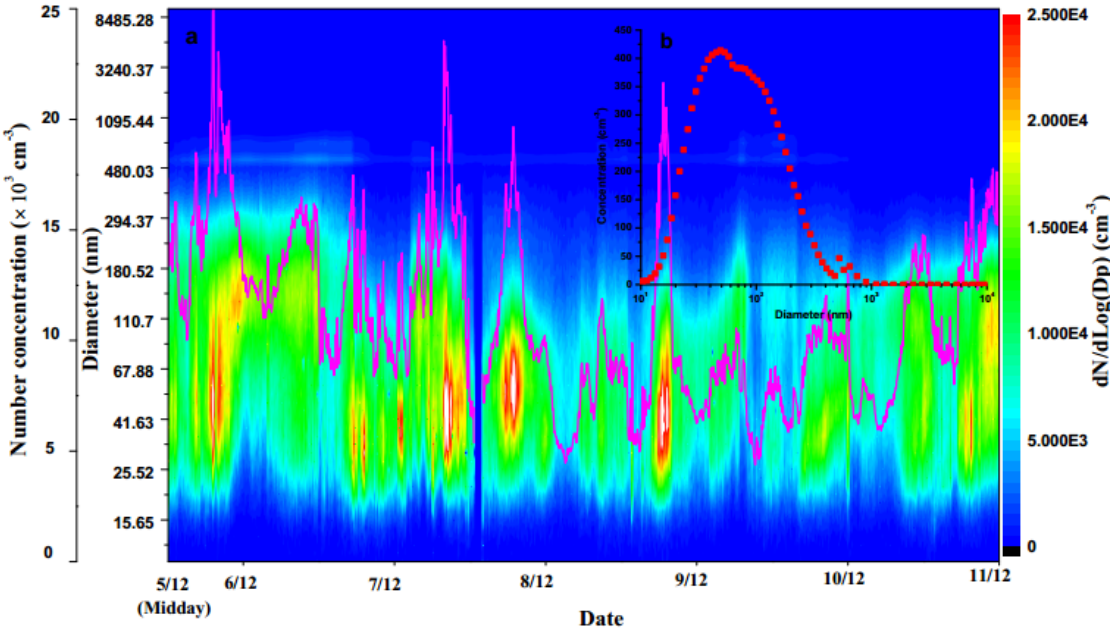

Figure 5 Time series of 4-min mean aerosol number size spectra and integrating number concentration (pink line, a) and averaged aerosol number size distribution (b) from 5 to 10 December 2013.

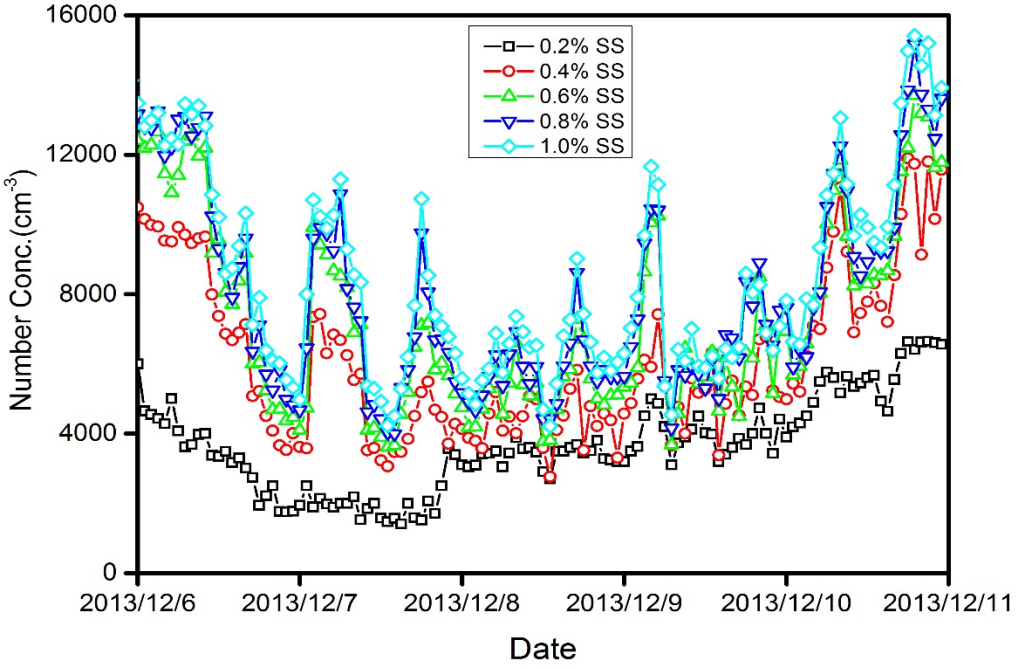

Figure 6 Time series of 1 h mean CCN concentration (N_{CCN}) at supersaturations (SS) of 0.2-1.0% from 6 to 10 December.

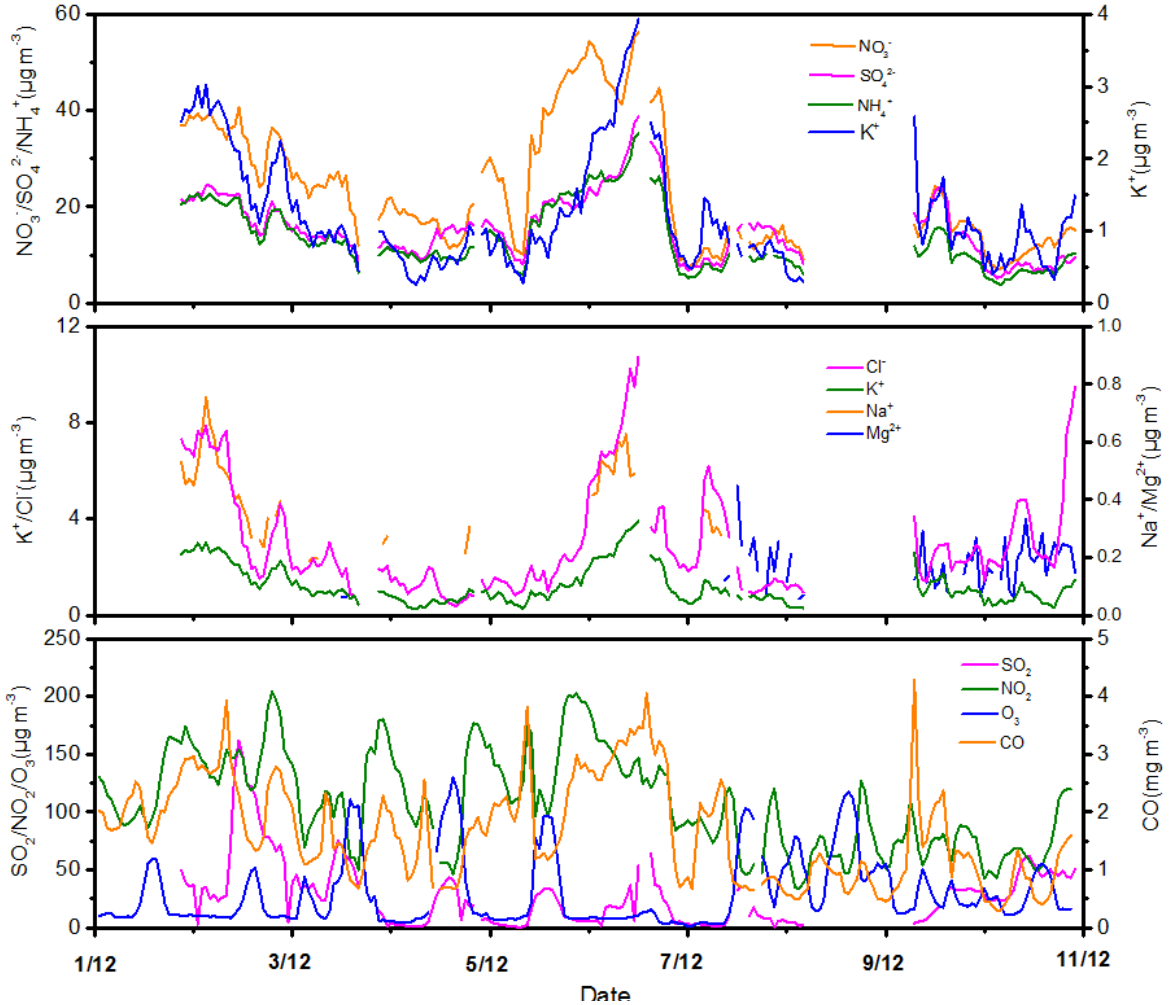

Figure 7 Temporal variations of chemical species in particles from 1 to 10 December 2013.

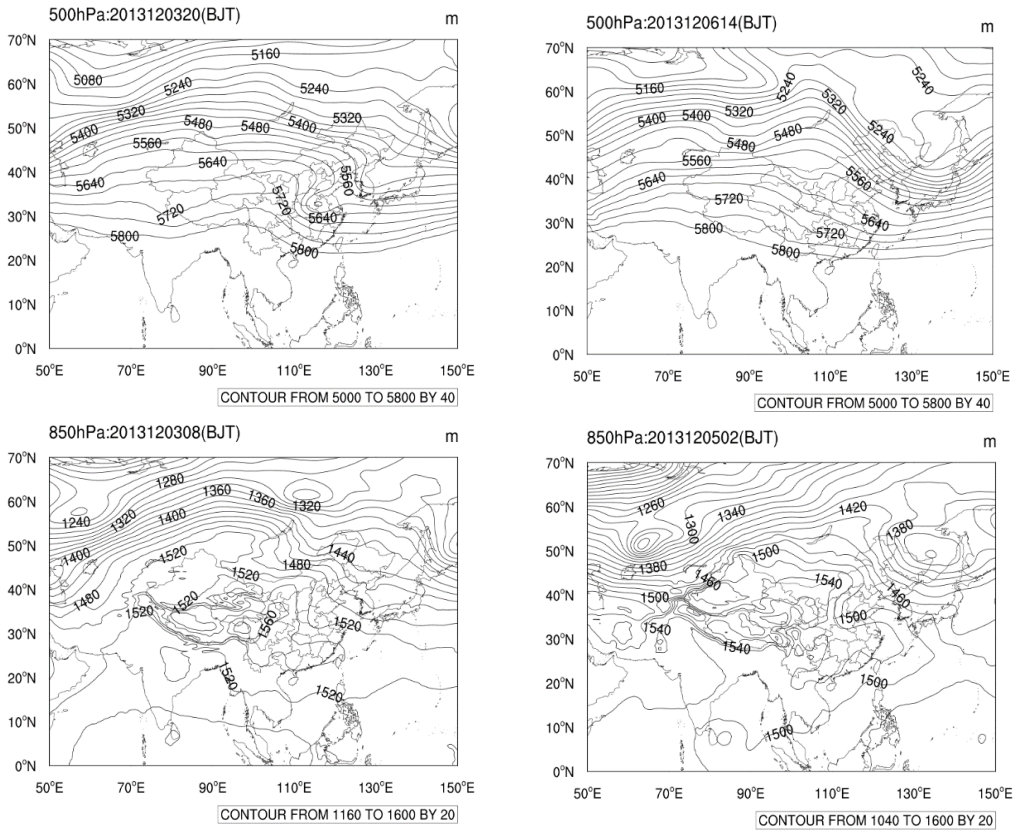

Figure 8 Atmospheric circulation situation at 500 hPa and 850 hPa from 3 to 6 December 2013.

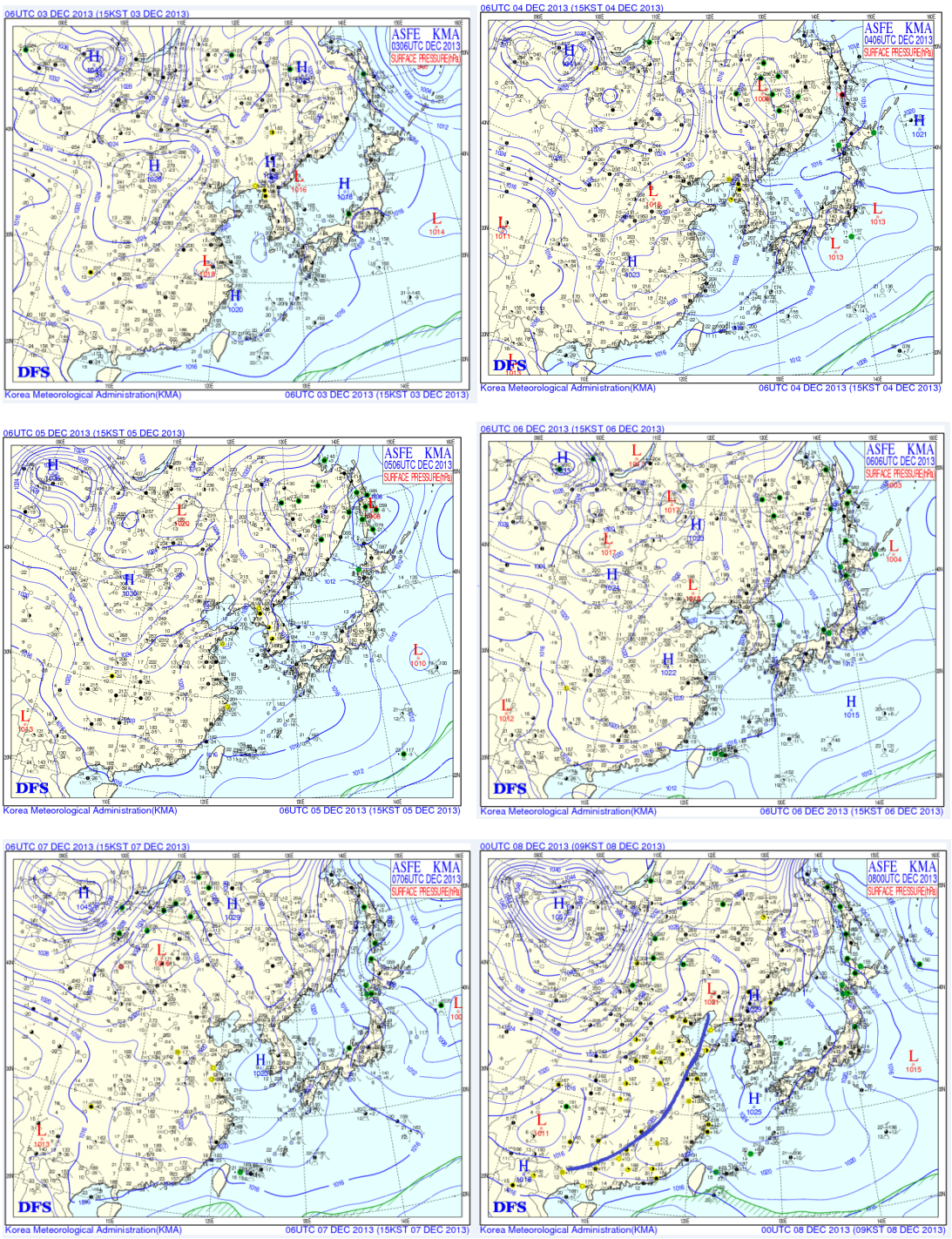

Figure 9 Surface weather maps at 6:00 (UTC) from 3 to 8 December 2013. The black star denotes the measurement site (http://qixiangxinxifabupingtai.ejinqiao.com).

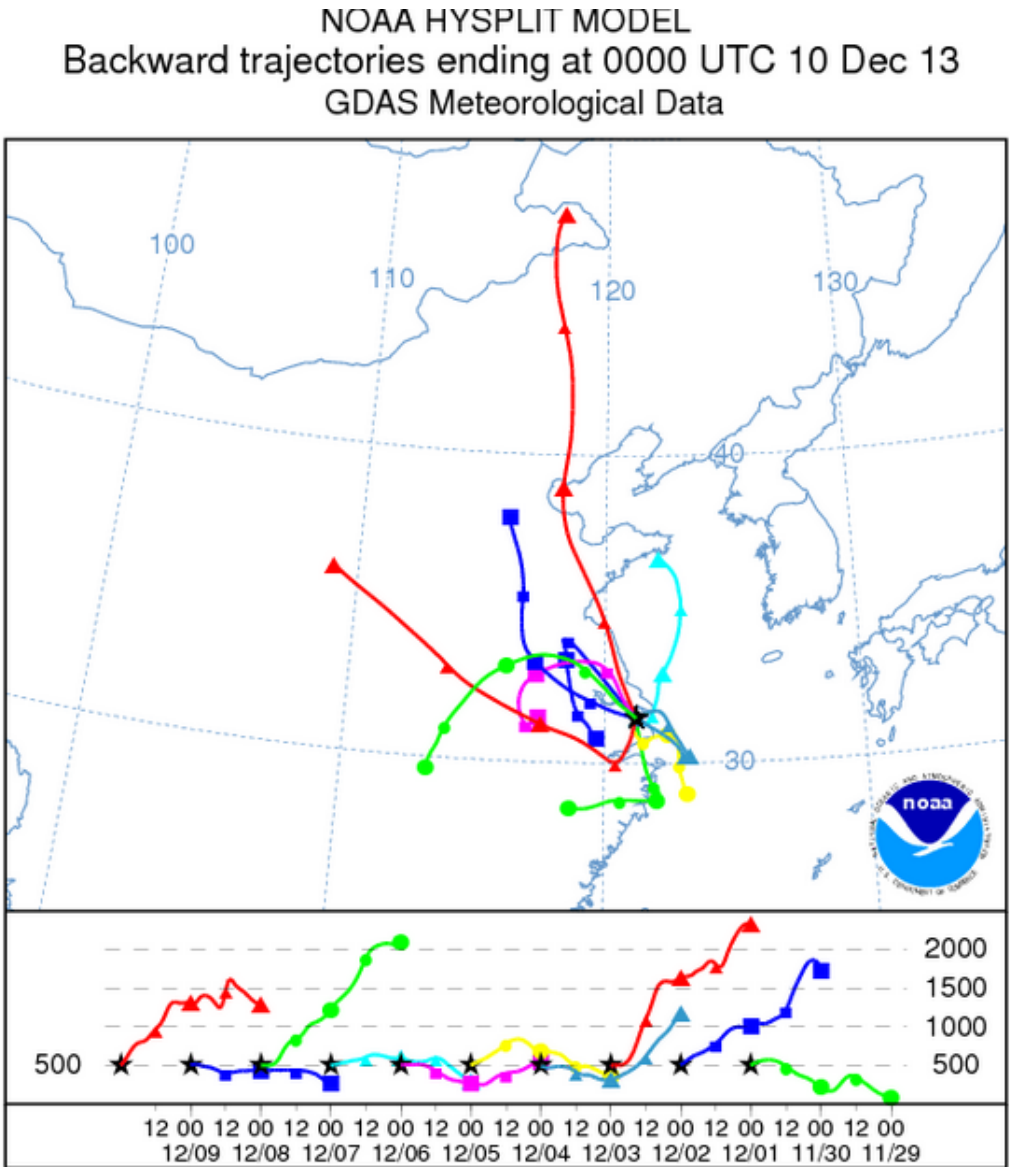

Figure 10 Air mass 48-h backward trajectories arriving at Shanghai from 1 to 10 December 2013 (500 m). A new trajectory is started at 0:00 (UTC) and calculated every 24 h.

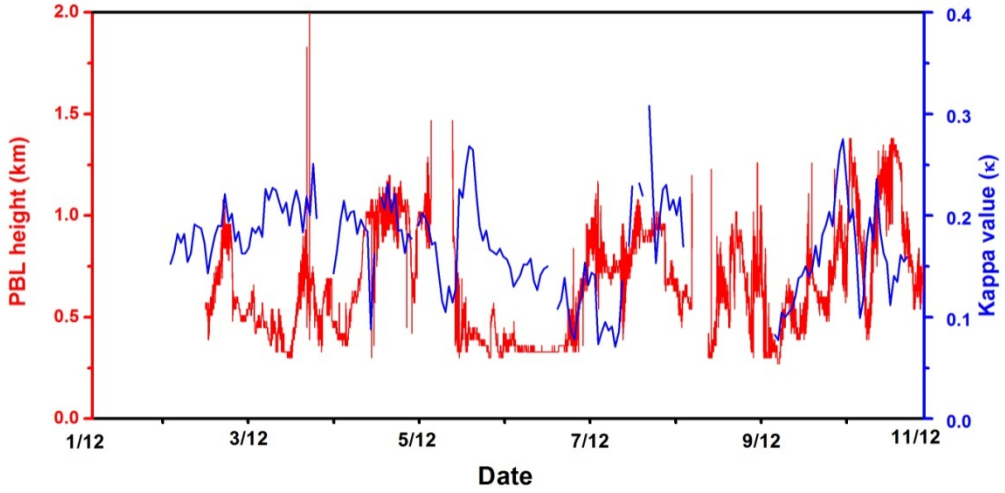

1062

1063 Figure 11 Time series of 1-h mean kappa value (i.e. κ) and 5-min mean

1064 PBL height from 1 to 10 December.

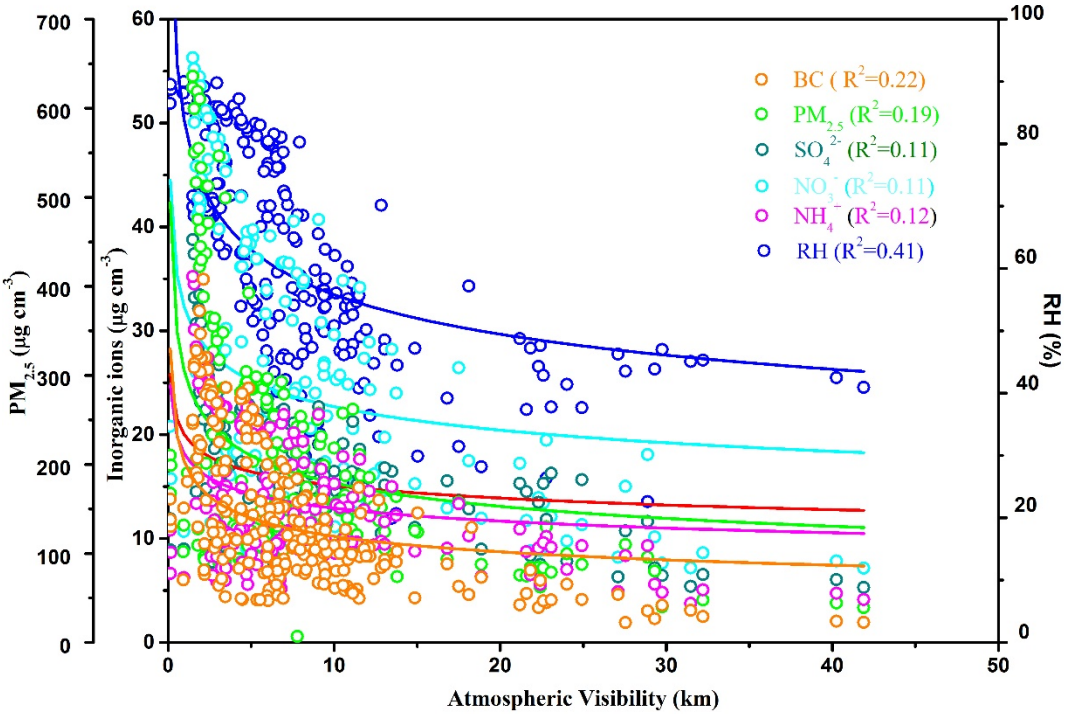

1065

1066 Figure 12 Scatter plots of RH, BC, $PM_{2.5}$ and inorganic ions in particles

1067 versus atmospheric visibility.

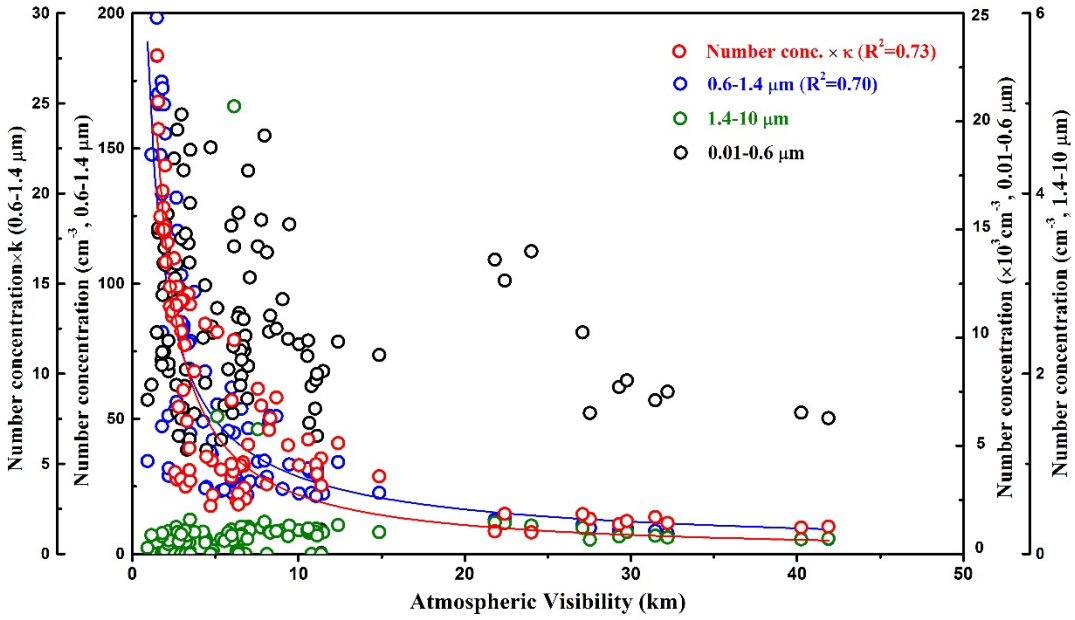

Figure 13 Scatter plots of aerosol number concentrations in ranges of 0.01-0.6 μm, 0.6-1.4 μm and 1.4-10 μm, and aerosol number concentration（0.6-1.4 μm） multiplied by particle hygroscopicity (kappa value, κ) versus atmospheric visibility.